—Headline—

Development of Lithium Iron Oxide Cathode Materials for Lithium Secondary Batteries

Yun -S. LEE,[a] Sung -J. CHO,[a] Yang -K. SUN,[b] Koichi KOBAYAKAWA,[c] and Yuichi SATO*[c]

[a]Faculty of Applied Chemical Engineering, Chonnam National University (300 Yongbong-dong, Kwangju 500-757, Korea)
[b]Department of Chemical Engineering, Hanyang University (17 Haengdang-dong, Seoul 133-791, Korea)
[c]Department of Applied Chemistry, Kanagawa University (3-27-1 Rokkakubashi, Kanagawa-ku, Yokohama 221-8686, Japan)

Received June 10, 2005 ; Accepted August 2, 2005

Two lithium iron oxides have been synthesized at low temperatures by the conventional solid-state method. Orthorhombic $LiFeO_2$ has been synthesized using LiOH and γ-FeOOH at 150℃ was composed of orthorhombic $LiFeO_2$ and small amount of spinel $LiFe_5O_8$ phases. A Li/$LiFeO_2$ cell showed not only a fairly high initial discharge capacity of over 150 mAh g^{-1} but also a good cycle retention rate at room temperature. It was found that the orthorhombic phase of the $LiFeO_2$ underwent a structural change to the $LiFe_5O_8$ spinel phase in the first cycle. Especially, it showed a severe structural change during the first discharge process, which might be the main reason for the capacity loss of the Li/$LiFeO_2$ system. An amorphous-like $Li_xFe_yO_z$ has been synthesized using LiOH and α-FeOOH at 200℃ consisted of three kinds of structures, $LiFe_5O_8$, Li_5FeO_4, and a trace of cubic α-$LiFeO_2$. A Li/$Li_xFe_yO_z$ cell showed a very high initial discharge capacity (215 mAh g^{-1}) as well as an excellent cycle retention rate (95%) from the 11th to the 50th cycle. It was found that $Li_xFe_yO_z$ material was transformed into the spinel $LiFe_5O_8$ and tetragonal β-$LiFeO_2$ phases after long-term cycling.

Key Words : Lithium Iron Oxide, Solid-state Method, Structural Transformation, Spinel $LiFe_5O_8$, Tetragonal $LiFeO_2$

1 Introduction

The battery industries have aimed to supply safe power sources with high energy density and good cycle performance. Lithium secondary batteries are the most promising candidate among the many possibilities to satisfy this demand. Many research groups have focused on the development of new cathode materials for lithium secondary batteries to realize the production of secondary batteries with high energy density.

Among the various cathode materials, the layered oxide materials, $LiMO_2$(M = Co, Ni, Mn, Fe···.), have been investigated as prospective cathode materials for lithium secondary batteries. Although $LiCoO_2$ is currently used as a cathode material of the commercial lithium ion battery, it involves many problems such as high cost, environmental aspects and low practical capacity (about 130 mAh g^{-1}).[1-2] $LiNiO_2$ has a larger practical capacity than $LiCoO_2$; however, it is highly possible for exothermic decomposition of the oxide to occur releasing oxygen at high temperature.[3-4] Recently, Li_xMnO_2 and $LiMn_{0.5}Ni_{0.5}O_2$ have been widely investigated because of their cost performance, environmental merit and easy preparation method compared with other cathode materials.[5-6]

$LiFeO_2$ also has many advantages over the above layered cathode materials because iron is nontoxic and one of the most abundant metals in the world. It is well-known that $LiFeO_2$ material has different types, α-, β-, and γ-forms, due to the synthetic condition and synthetic method. α-$LiFeO_2$ is a cubic unit cell of space group Fm 3m, and β-$LiFeO_2$ (tetragonal, $I4_1$/amd or monoclinic, C 2/c) is formed into an intermediate phase during the ordering process. γ-$LiFeO_2$ (tetragonal, $I4_1$/amd) is obtained by reducing the symmetry from cubic to tetragonal by ordering Li^+ and Fe^{3+} ions at octahedral sites.[7-15]

Kanno *et al*. found that a corrugated layered structure $LiFeO_2$ compound was electrochemically active during the lithium insertion/extraction reaction.[7-8] They noticed one interesting point that orthorhombic $LiMnO_2$ formed using LiOH and γ-MnOOH, which has a structure similar to that of conjugated $LiFeO_2$, was synthesized successfully by an ion exchange method at low temperature.[16-17] They succeeded in synthesizing $LiFeO_2$ material using the H^+/Li^+ ion exchange reaction from γ-FeOOH at a reaction temperature of 100 to 500℃. Although this Li/$LiFeO_2$ cell exhibited a fairly high initial discharge capacity of about 100 mAh g^{-1} and lithium was reversibly inserted/extracted in the FeO_2 layers, it showed a large capacity decline due to the cationic disorder in the voltage region of 4.2 and 1.5 V.

Tabuchi *et al*. announced many interesting results for all types of $LiFeO_2$ compounds.[9-13] They successfully adopted a new synthetic process, a hydrothermal method, for the $LiFeO_2$ system. Many kinds of starting materials (α-FeOOH, $FeCl_3$, $Fe(NO_3)_3$, LiOH, NaOH, and KOH) at

Table 1 Properties and polymorphs of lithium iron oxides.

phase	Crystal structure		Unit-cell parameter	Ref.
α-$LiFeO_2$	cubic	Fm3m	a = 4.158 Å	PDF # 17-0938
β-$LiFeO_2$	tetragonal	$I4_1/amd$	a = 4.152 Å, c = 4.920 Å	
	monoclinic	C2/c	a = 8.571 Å, b = 11.589 Å, c = 5.147 Å, β = 145.7°	
γ-$LiFeO_2$	tetragonal	$I4_1/amd$	a = 4.05 Å, c = 8.74 Å	PDF # 17-0937
α-$LiFe_5O_8$	cubic	$P4_132$	a = 8.3313 Å	PDF # 49-0266
β-$LiFe_5O_8$	cubic	Fd-3m	a = 8.390 Å	PDF # 74-1911
Corrugated $LiFeO_2$	orthorhombic	Pnma	a = 9.677 Å, b = 2.934 Å, c = 5.005 Å	PDF # 52-0698
Li_5FeO_4	orthorhombic	Pbca	a = 9.218 Å, b = 9.213 Å, c = 9.159 Å	PDF # 75-1253

various Li/Fe (1-50) ratios were distilled in a Teflon beaker and hydrothermally treated at 230℃ in an autoclave. Although α-$LiFeO_2$ derivatives were successfully obtained between α-FeOOH (Fe^{3+} source) and LiOH by a one-step method, the cycling performance of the α-$LiFeO_2$ compound was very poor (5-10 mAh g^{-1}) in the range 4.5 to 1.5 V. Properties and polymorphs of conventional lithium iron oxides were shown in Table 1.

Furthermore, Kim and Manthiram reported that a nano-crystalline lithium iron oxide ($Li_xFe_yO_z$) of an amorphous type presented a high discharge capacity of about 140 mAh g^{-1} with a fairly good cycleability in the range of 1.5 and 4.3 V. They have synthesized various kinds of lithium iron oxides with a Li/Fe ratio of 0.69-1.22 using the solution method, which utilized the oxidation reaction of Fe^{2+} with lithium peroxide in the presence of excess lithium hydroxide in aqueous medium.[18] Although they successfully obtained a lithium iron oxide with a fairly good battery performance at low temperature (200℃), the cycle characteristics and synthetic method, due to the excess use of the lithium source by the solution method, are still unsatisfactory for use as a practical cathode material for lithium secondary batteries.

From a review of previous studies, we found that almost all conventional lithium iron oxide materials were obtained using complex reaction mechanisms (*e.g.*, an ion exchange reaction, a hydrothermal method, and a wet solution method). A long reaction time was needed or other reaction steps compared to the conventional solid-state method. Moreover, almost all lithium iron oxide materials using the above methods were unsatisfactory as a practical cathode material, from the viewpoint of the reversible discharge capacity and cycling performance, in lithium secondary batteries.

Therefore, we report here new and easy synthetic methods of orthorhombic $LiFeO_2$[19-20] and amorphous-type $Li_xFe_yO_z$[21] cathode materials with good battery performances using a conventional solid-state reaction at low temperatures (150 or 200℃). Furthermore, we also suggest the capacity loss mechanism and the unique structural changes in lithium iron oxide system.

2 Experimental

Lithium iron oxides were synthesized at various calcination temperatures by the solid-state method. Orthorhombic $LiFeO_2$ material was synthesized using LiOH · H_2O (Kishida Chemical, Japan), and γ-FeOOH (High Purity Chemicals, Japan). A stoichiometric amount of each material was ground and calcined at 150℃ for 15 h in Ar atmosphere in a box furnace. One mixture was calcined in a ceramic boat without pressing; the other was pressed at a 300 kg cm^{-2} pressure into a 20 mm diameter pellet to improve the reactivity between particles of the precursor. Amorphous $Li_xFe_yO_z$ material was synthesized using LiOH · H_2O (Aldrich Chemical, USA), and α-FeOOH (Aldrich Chemical, USA) by the solid-state method. A stoichiometric amount of each material was thoroughly ground in a mortar for 1 h, and the mixture was calcined at 200-800℃ for 12 h in N_2 atmosphere. The contents of Li and Fe in the resulting materials were analyzed by atomic absorption spectroscopy (AAS, AA-6200, Shimadzu, Japan) by dissolving the powder in dilute nitric acid.

Powder X-ray diffraction (XRD, Rint 1000, Rigaku, Japan) using CuKα radiation was employed to identify the crystalline phase of the synthesized material. To investigate the structural change in the positive electrode during cycling, *in-situ* XRD measurements were conducted using a homemade cell.[22] Cell assembling and handling during the *in-situ* XRD measurements were done in an argon-filled glove box to prevent any reaction with moisture in the air. After reaching the desirable voltage point, the *in-situ* XRD cell was left in the glove box for 6 hrs to reach equilibrium during the entire measurement. Additionally, in order to investigate the cycling behavior after long-term cycling, *ex-situ* XRD measurements were conducted on the cycled electrodes after various cycles. Each cell was left in the glove box for 2 days to reach equilibrium after being tested from 1.5 V to 4.5 V.

To detect a structural change, a vibrational sample magnetometer (VSM, Riken Denshi, Japan) was used for collecting the magnetic field dependence of magnetization (*M-H*) data at 300 K. Magnetization curves were measured between −10 and +10 kOe. A transmission electron microscope (TEM, JEM 2010, JEOL, Japan) equipped with an energy-dispersive x-ray spectrometer (EDS) was also employed to characterize the microstructure of the powder.

The electrochemical characterizations were performed using a CR 2032 coin-type cell. The cathode was fabricated of 20 mg of accurately weighed active material, 12 mg of conductive binder (8 mg of Teflonized acetylene black (TAB) and 4 mg of graphite). The mixture was pressed on a 200 mm^2 stainless steel mesh used as the current collector under a pressure of 300 kg cm^{-2} and

dried at 130℃ for 5 h in an oven. The test cell was made of a cathode and a lithium metal anode (Cyprus Foote Mineral Co.) separated by a porous polypropylene film (Celgard 3401). The electrolyte used was a mixture of 1 M $LiPF_6$-ethylene carbonate (EC)/dimethyl carbonate (DMC) (1:2 by vol., Ube Chemicals, Japan). The charge/discharge current density was 0.1 mA cm^{-2} with a cutoff voltage of 1.5 to 4.5 V at room temperature.

3 Results and Discussion

3. 1 Preparation and electrochemical characterization of Li/$LiFeO_2$ system

Figure 1 shows x-ray diffraction (XRD) patterns of the raw γ-FeOOH and the two $LiFeO_2$ materials which were calcined at 150℃ for 15 h in Ar atmosphere. The $LiFeO_2$ mixture without pressing (Fig. 1(b)) shows a very similar XRD pattern compared to the γ-FeOOH. It seems to fail to form an orthorhombic structure, although there are some differences from that of the original γ-FeOOH, which resulted from the reaction with lithium hydroxide at 80℃. On the other hand, Fig. 1(c) displays a well-defined orthorhombic pattern in the XRD diagram. The characteristic indications of orthorhombic $LiFeO_2$ (herein referred to as o-$LiFeO_2$) material are well defined by the concrete split between the (011) and (110) peaks and between the (012) and (200) peaks, although there are small amounts of β-$LiFe_5O_8$ impurities. We found that the pelletizing in this study played an important role in accelerating the slow reaction of lithium and γ-FeOOH particles because the rate of surface reaction of the two starting materials was slow at the low synthetic temperature.

Figure 2 shows the transmission electron microscope (TEM) bright field image and selected area electron diffraction (SAD) patterns of the o-$LiFeO_2$ material. All of the electron diffraction patterns were obtained from the o-$LiFeO_2$ particles in this study. This shows that the $LiFeO_2$ sample consisted of 100-200 nm sized needle-type particles. It is composed of an orthorhombic phase (a = 4.0 Å, b = 3.0 Å, and c = 6.1 Å) with a small amount of β-$LiFe_5O_8$ (cubic, a = 8.3 Å) phase (Fig. 1(c)). Additionally, some of the orthorhombic phases (Fig. 2(d)) had a different stacking sequence in the c-direction, giving rise to a superlattice peak. White arrows indicate the spots arising from the superlattice generated by the altered stacking sequence in the c-direction as shown above. We assume that the altered stacking sequence and higher amount of the spinel phase have combined to decrease the discharge capacity of the $LiFeO_2$ material. From the TEM analysis, the $LiFeO_2$ in this study was found to be mixed with well-crystallized orthorhombic $LiFeO_2$, cubic β-$LiFe_5O_8$, and defective $LiFeO_2$ phases.

Figure 3(a) exhibits the charge/discharge curves for Li/1 M $LiPF_6$-EC/DMC/o-$LiFeO_2$ calcined at 150℃ for 15 h in argon. The test condition was a current density of 0.1 mA cm^{-2} between 4.5 and 1.5 V. The voltage during the first charge of the Li/o-$LiFeO_2$ cell increased rapidly to 4.0 V and showed a plateau region between 4.2 and 4.3 V. The first discharge curve abruptly decreased to below 3.0 V and displayed a voltage plateau of 2.0-2.1 V region followed by two more small voltage steps. In the second cycle, the plateau region at the 2.0 V region was not detected and it exhibited a slightly different cycle behavior. This clearly exhibited that the Li/o-$LiFeO_2$ system presented fairly different cycle characteristics from the second cycle during further cycling. The initial discharge capacity of the Li/o-$LiFeO_2$ cell in this study was 150 mAh g^{-1}, which was one of the largest values as reported previously. We assume that the large discharge capacity of the Li/o-$LiFeO_2$ cell in this study might result from the absence (or scarcity) of the inactive α-$LiFeO_2$ impurity in the $LiFeO_2$ structure.

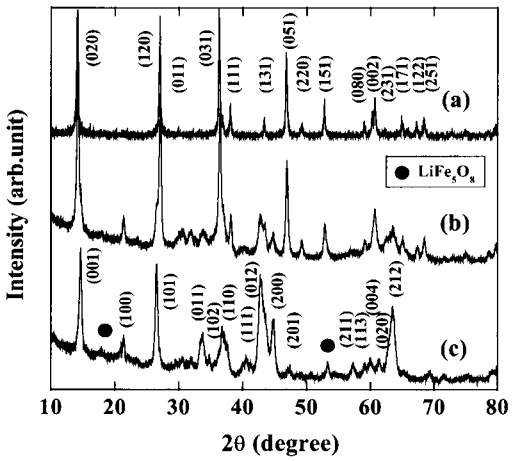

Fig. 1 X-ray diffraction patterns of (a) γ-FeOOH, (b) $LiFeO_2$ without pressing, and (c) $LiFeO_2$ with pressing.

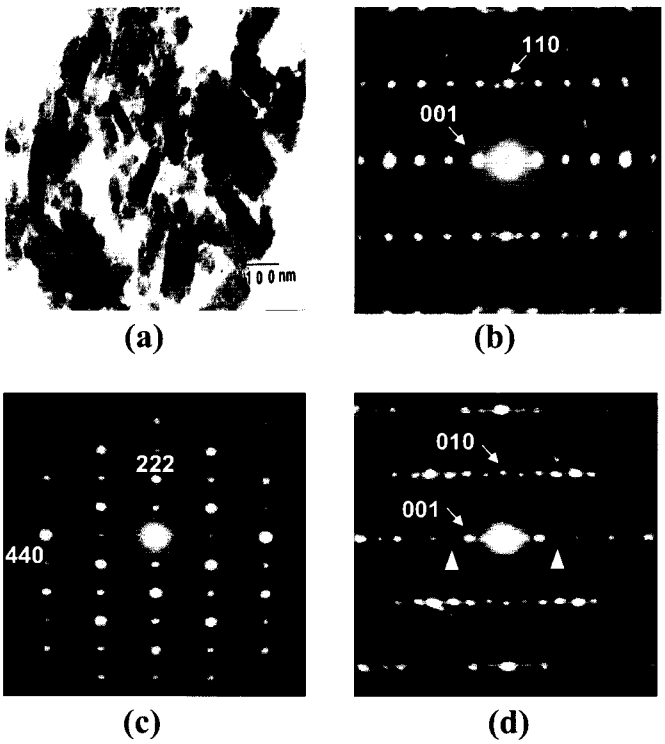

Fig. 2 TEM image and SAD patterns of the resulting powder. (a) bright field image of orthorhombic $LiFeO_2$, (b) orthorhombic $LiFeO_2$ in the [110] direction, (c) spinel β-$LiFe_5O_8$ in the [112] direction, and (d) defective $LiFeO_2$ in the [100] direction.

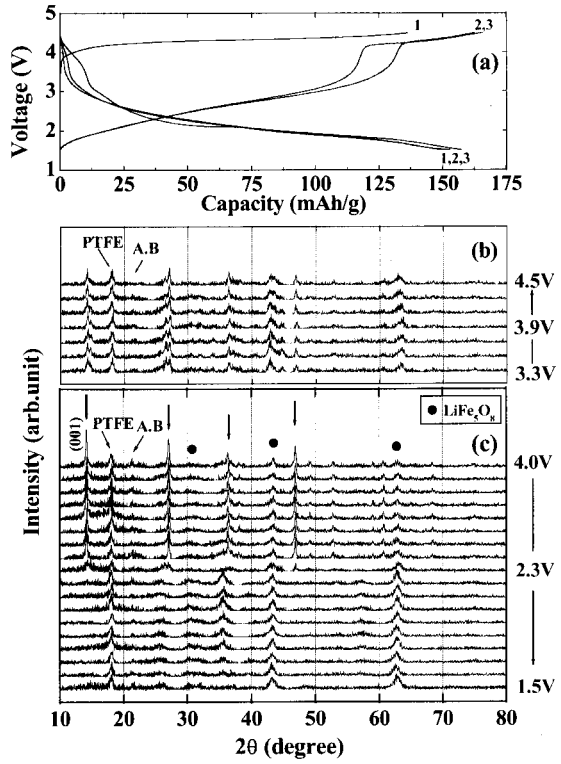

Fig. 3 (a) The charge/discharge curves for the Li/1 M $LiPF_6$-EC/DMC/$LiFeO_2$ cell with material calcined at 150℃ and *in-situ* XRD patterns for the this cell during (b) the 1st charge, and (c) the 1st discharge process. The test condition was a current density of 0.1 mA/cm^2 between 4.5 and 1.5 V at room temperature.

To investigate the difference on cycling between the first and second (third) cycles, *in-situ* XRD of the Li/*o*-$LiFeO_2$ cell was conducted using a homemade *in-situ* XRD cell. The counter and reference electrodes were prepared by pressing lithium foil onto a stainless steel mesh. The cell construction of the *in-situ* XRD cell was described in our previous report.[22] The test condition was the same as the cycling test at a current density of 0.1 mA cm^{-2} between 4.5 and 1.5 V. Figure 3(b) shows the *in-situ* XRD patterns of the Li/*o*-$LiFeO_2$ cell during the first charge process. As expected from the smooth voltage plateau in the charge curve, the *in-situ* XRD during the first charge process showed no big difference in the whole XRD diagram, although some peaks are split into two parts during charge and other peaks are slightly intensified according to the depth of charge. However, Fig. 3(c) shows clearly the many peak changes of the Li/*o*-$LiFeO_2$ cell during the first discharge process. The main orthorhombic peak at $2\theta = 14.6°$ was maintained to 2.4 V; however, it significantly decreased during the 2.3 V region, and this clear (001) peak could not be detected after this point. Moreover, other major peaks also started to change in the 2.3 V region. Some of the major peaks will diminish during deep lithium insertion into the Li_xFeO_2 structure, while the other small peaks of $2\theta = 43°$ or $63°$ (mainly the spinel phase), in contrast to the strong major peaks, become the stronger peaks in the deep discharge state. Although the perfect cubic spinel

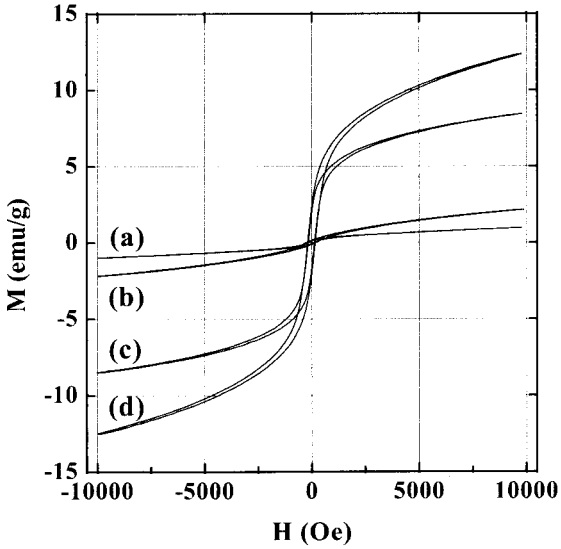

Fig. 4 Field dependence of the magnetization of various materials and electrodes. (a) cubic α-$LiFeO_2$, (b) orthorhombic $LiFeO_2$, (c) the 1st charged state, and (d) the 1st cycled state of an orthorhombic $LiFeO_2$ electrode.

$LiFe_5O_8$ phase still failed to appear in this XRD diagram, the XRD pattern at 1.5 V is very similar to that of the cubic $LiFe_5O_8$ and starts to show the (220) peak of the $LiFe_5O_8$ spinel at $2\theta = 31°$ during the first discharge.

However, it still needs to define the real remaining phase in/onto the electrode after the first cycle, because some peaks in the XRD patterns after the first charge/discharge process in Fig. 3 (b,c) are also partially similar to those of α and β-$LiFeO_2$ phases, such as the (200) and (220) peaks of α-$LiFeO_2$ (see Fig 7(d)). To confirm the remaining phase in/onto the electrode, the magnetic properties of each sample (α-$LiFeO_2$, *o*-$LiFeO_2$, charged and discharged electrodes) were examined using a VSM at room temperature. Because all conventional $LiFeO_2$ shows antiferromagnetic ordering below room temperature, the magnetic field (H) dependence of the magnetization (M) for the above samples could successfully detect a magnetic impurity such as $LiFe_5O_8$ in/onto the powders and electrodes after the charge and discharge process.

Figure 4 shows the field dependence of the magnetization of various $LiFeO_2$ powders and electrodes after cycling. Unfortunately, the α-$LiFeO_2$ powder in this study shows no ideal behavior in the M/H loop test, due to the small amount of impurity, which was obtained by the hydrothermal method (Ref. Tabuchi *et al*. *J. Solid State Chem*., **140**, 159 (1998)). It is well-known that the hydrothermal method sometimes involves difficulty in obtaining a single-phase compound, because it uses many reaction steps and other chemicals during the synthetic process. As described before, the orthorhombic $LiFeO_2$ material in this study was composed of an orthorhombic phase, a small amount of β-$LiFe_5O_8$, and defective $LiFeO_2$. The result of the M-H test for orthorhombic $LiFeO_2$ powder showed a slightly shaped pattern due to the existing $LiFe_5O_8$ phase (about 1%) in the structure, and the pattern of the M/H curve was fairly similar to

that of α-$LiFeO_2$ with a small amount of impurity. The weight fraction of β-$LiFe_5O_8$ (M_s=65 emu g^{-1} at 300 K) in each sample was estimated as the ratio of the observed spontaneous magnetization, M_s (0.884(5) emu g^{-1}) to that of the above magnetic impurity. The M_s value was calculated as an average of extrapolated data at $H=0$ from two least square lines consisting of M-H data more than 5 kOe or less than 5 kOe. On the other hand, the electrodes after charge and discharge clearly reveal the structural change in the Li/o-$LiFeO_2$ cell cathode during the first cycling. In the case of the electrode after the charge process, it clearly shows the S shape of the conventional $LiFe_5O_8$ phase in the M-H test. The value of the spontaneous magnetization of this electrode is 6.443(2) emu g^{-1}. Moreover, the electrode after the first cycle exhibits a more developed S shape than that after the first charge. The value of magnetization for the electrode after the first cycle is 8.68(2) emu/g.[13] This means that the electrode after the first cycle has a larger amount of the spinel $LiFe_5O_8$ phase than that of an electrode after the first charges, and it also explains clearly that the phase change, from the orthorhombic $LiFeO_2$ to the spinel $LiFe_5O_8$, is accelerated as the cycling proceeds. Based on these results, we could consider that the orthorhombic $LiFeO_2$ underwent severe structural changes during the first cycle, which induced a structural change from the orthorhombic to the spinel phase.

Figure 5 shows the cycle characteristics of the Li/o-$LiFeO_2$ cell in long-term cycling at room temperature. The test condition was a current density of 0.1 mA cm^{-2} between 4.5 and 1.5 V. This Li/o-$LiFeO_2$ cell shows a slightly increased discharge capacity up to the 3rd cycle and maintains a stable cycle performance between the 15 th and 50th cycles. The cycle retention rate of Li/o-$LiFeO_2$ cell was above 70% after 50 cycles, which was one of the highest values in the lithium iron oxide system.

However, it occurred to us how changed spinel phase could maintain (or develop) into the following cycles? In order to investigate the further structural change in the long-term cycling, $LiFeO_2$ electrodes in the discharged state after 3rd (the maximum point of discharge capacity) and 50th cycles were taken from the test cells in the glove box. The electrodes were washed with DMC solution to remove $LiPF_6$ salt and left in a glove box for 2 days to reach equilibrium after being tested from 1.5 to 4.5 V. Figure 6 shows the TEM bright field image and electron diffraction patterns of the o-$LiFeO_2$ electrodes after the 3rd and 50th cycles. As can be seen from the indexed polycrystalline ring pattern(Fig. 6 (a,b,c)), nearly all of the initial o-$LiFeO_2$ phase was converted into the spinel phase after just one cycle, as almost no trace of o-$LiFeO_2$ was observed using TEM analysis. A well-developed spinel structure was evidenced from the single crystal diffraction pattern in the [110] zone obtained from one of the particles in the cycled electrode. The diffraction pattern well matched that taken from a perfect spinel $LiFe_5O_8$ structure. After further cycling the electrode for 50 cycles (Fig. 6 (d,e,f)), no significant structural changes were observed from the TEM analysis. Comparing the bright field images after the 3rd and 50th cycles, the particle size and morphology are quite similar, indicating that no further serious structural transformations occurred after the first few cycles. The polycrystalline ring pattern and single crystal pattern in the [100] zone taken after 50 cycles also shows that the spinel $LiFe_5O_8$ structure was well maintained during the subsequent cycles after the initial structural transformation. One difference between the two electrodes was that the electrode after 50 cycles showed a large amount of defects and underwent a more serious phase transformation to the spinel $LiFe_5O_8$ phase, due to the long-term cycling. The TEM analysis conclusively proved that the phase transition from the orthorhombic structure to the spinel structure of the Li/$LiFeO_2$ cell was almost completed after a few cycles and that during the subsequent charge/discharge process, the electrode underwent minimal structural change.

Based on these results from the *in-situ*, *ex-situ* XRD, and TEM measurements, it could be considered that the Li/o-$LiFeO_2$ cell underwent severe structural changes into the spinel $LiFe_5O_8$ form during the early stage and continued the transformation into the spinel $LiFe_5O_8$ phase during the long-term cycling.

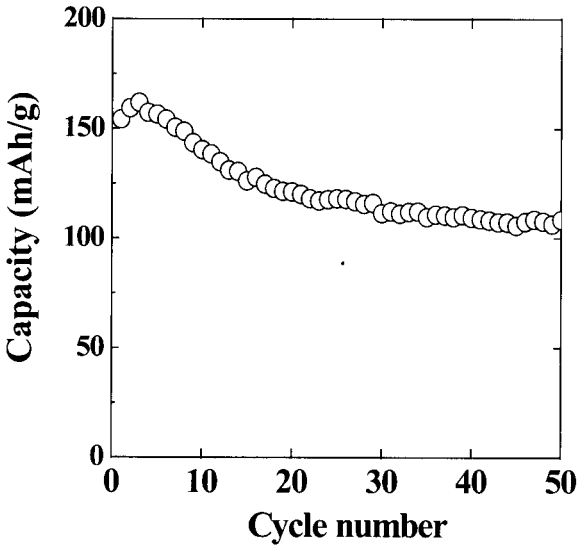

Fig. 5 A plot of the specific discharge vs. number of cycles for the Li/1 M $LiPF_6$-EC/ DMC/$LiFeO_2$ system with material calcined at 150℃.

3. 2 Synthesis and structural change of $Li_xFe_yO_z$ with amorphous structure

Figure 7 shows the XRD patterns of the resulting powders calcined at various temperatures. The lithium iron oxide obtained at 200℃ (Fig. 7(a)) showed a broad reflection pattern, which was made up of a polymorphous structure with poor crystallinity, small particle sizes, and an amorphous-like phase. The intermediate compounds (300℃ and 400℃) were gradually transformed into a mixture of the $LiFe_5O_8$, Li_5FeO_4, and a trace of cubic α-$LiFeO_2$ phases. Additionally, the XRD pattern obtained at 400℃ exhibited stronger α-$LiFeO_2$ main diffraction peaks, such as (111), (200), and (220), than those of the 300℃ sample. Moreover, the compound obtained at

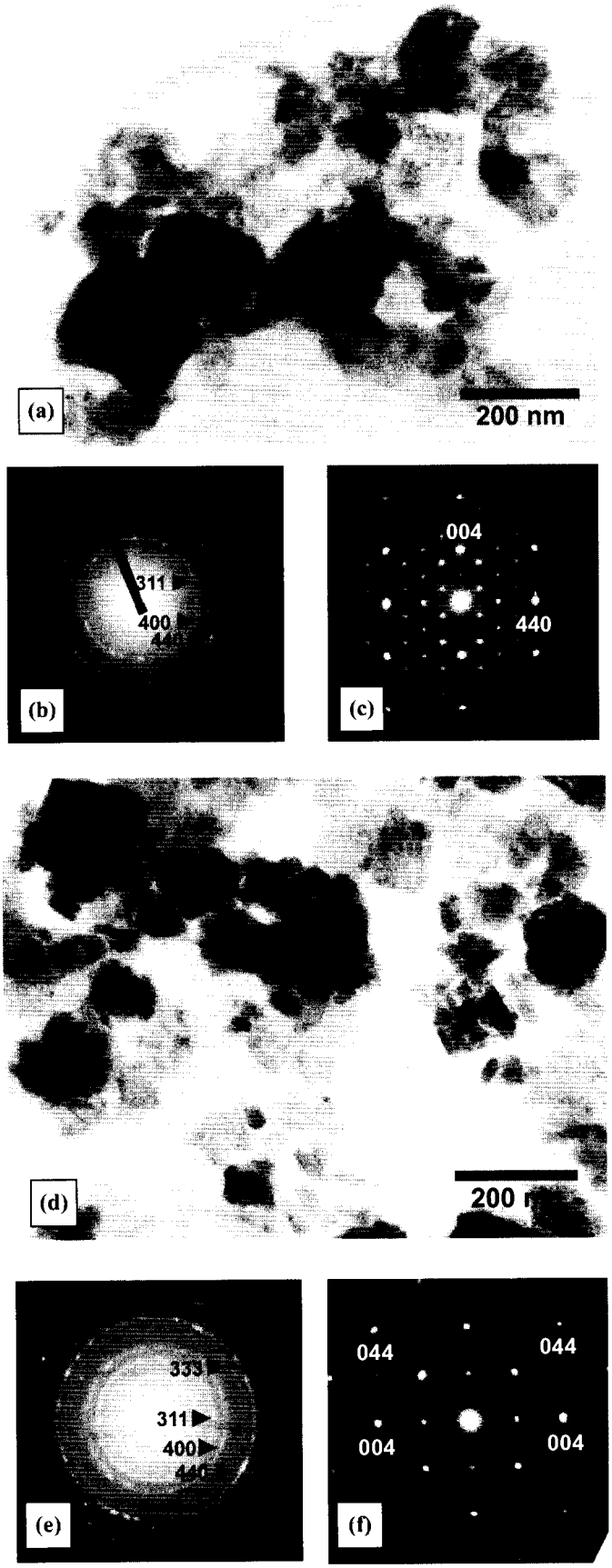

Fig. 6 TEM image and SAD patterns of electrodes after cycles (a,b,c) after the 3rd cycle, and (d,e,f) after the 50th cycle.

800℃ exhibited a single cubic α-$LiFeO_2$ phase, which is well-known to have difficulty inserting/extracting lithium into and out of its structure.

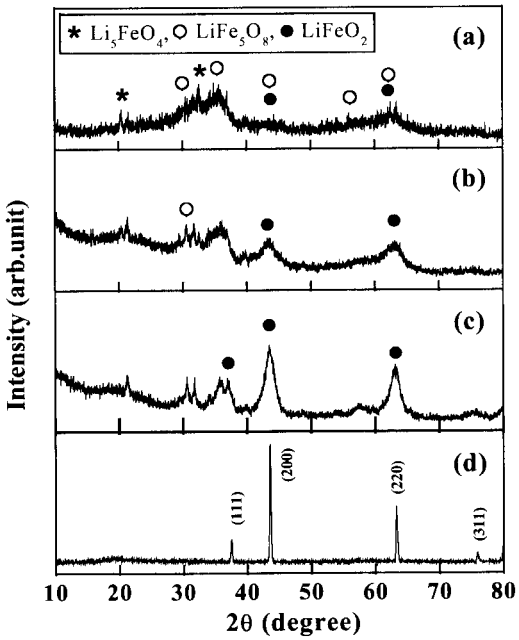

Fig. 7 X-ray diffraction patterns for $Li_xFe_yO_z$ powders obtained at (a) 200℃, (b) 300℃, (c) 400℃, and (d) 800℃.

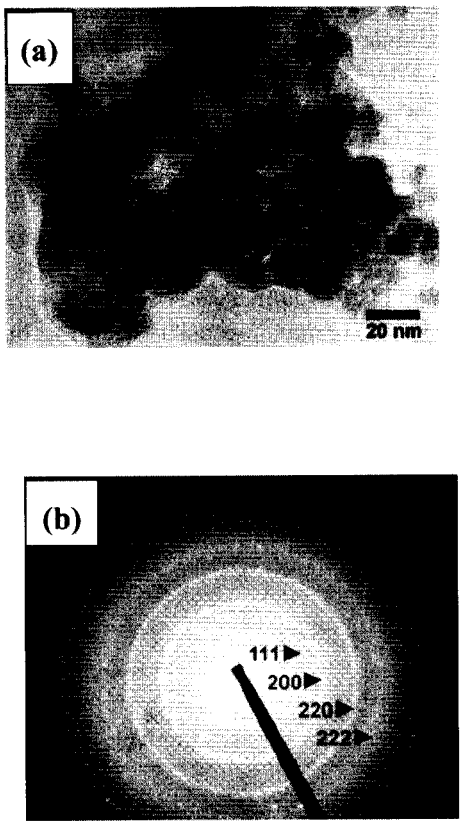

Fig. 8 TEM bright-field images of the $Li_xFe_yO_z$ powder obtained at 200℃. (a) magnified image and (b) polycrystalline electron diffraction pattern.

In order to investigate the original structure of lithium iron oxides, transmission electron microscopy analysis was performed. TEM bright-field images and an electron diffraction pattern for the lithium iron oxide obtained at 200℃ are shown in Fig. 8. The bright-field images show that the powder consists of an agglomeration of fine particles of less than 20 nm in size. In addition, the particle

shapes are not well-defined which suggests that the powder is poorly crystallized in agreement with the XRD result. The polycrystalline ring pattern shown in Fig 8(b) alone is sufficient to identify conclusively the structure of the $Li_xFe_yO_z$ powder partly due to the numerous polymorphs of lithium iron oxide. Two strong peaks, however, suggest that the as-prepared material has one of following cubic structures: α-$LiFeO_2$ (*Fm3m*), α-$LiFe_5O_8$ ($P4_132$, ordered high temperature phase), or cubic β-$LiFe_5O_8$ (*Fd3m*). The pattern in Fig 8(b) has been indexed based on the α-$LiFeO_2$ structure because of the absence of the strong (311) peak. The powder could well be a mixture of the different cubic phases.

Figure 9(a) shows the charge/discharge curves of the $Li/Li_xFe_yO_z$ cell obtained at 200℃. The charge/discharge current density was 0.1 mA cm^{-2} with a cut off voltage of 1.5 to 4.5 V at room temperature. The first charge curve of the $Li/Li_xFe_yO_z$ cell rapidly increased up to 4.0 V. This cell shows a small plateau region at about 4.1 V and exhibits another long voltage plateau between 4.2 and 4.3 V. While the first discharge curve drastically decreased to 3.3 V, it showed two small voltage plateaus between 2.0 and 1.5 V. For the second cycle, the voltage profile gradually decreased without any remarkable voltage plateau and exhibited a slightly different shape compared to that of the first cycle. Figure 9(b) exhibits the specific discharge capacity with the number of cycles for the $Li/Li_xFe_yO_z$ cell obtained at 200℃. This $Li/Li_xFe_yO_z$ cell presented a high initial discharge capacity of 215 mAh g^{-1} and an excellent cycle retention rate from the 11th to the 50th cycle. Although this material showed a slightly large capacity loss up to the 10th cycle, the cycle retention rate from the 11th to 50th cycle was 95%, which is the highest value as previously reported. On the other hand, we also found that there seemed to be one unique characteristic in Fig. 9(b). $Li_xFe_yO_z$ obtained at 200℃ showed a large capacity drop during the early stage and then maintained an excellent cycling performance up to 50 cycles. This indication might suggest that the $Li_xFe_yO_z$ powder obtained at 200℃ might have undergone a structural change in the early stage and that it had a high possibility of showing unique cycle characteristics like that of the Li/o-$LiFeO_2$ system.

In order to investigate this unique cycling behavior of $Li_xFe_yO_z$ obtained at 200℃, especially during the early stage, *ex-situ* XRD measurements were taken of four electrodes in the discharged state after various cycles. Figure 10 shows the results of the *ex-situ* XRD patterns after various cycles of the four electrodes, which remained in the glove box for 2 days to reach equilibrium after being tested from 1.5 V to 4.5 V. We tried to divide these *ex-situ* XRD results into two parts to easily explain the relation between the structural change and the cycling behavior, although this could be considered a gradual structural change from the 1st to the 50th cycle. One group (1st and 3rd cycles) presented almost the same XRD patterns, which is a mixture of cubic β-$LiFe_5O_8$ and a small amount of $LiFeO_2$ phase. Although it was difficult to clearly distinguish the type of $LiFeO_2$ phase between the α and β phases due to the low crystallinity and some impurities, the main common XRD peaks for two kinds of $LiFeO_2$ could be detected such as the (200) and (220) peaks of the α- and β-$LiFeO_2$ (α- : JCPDS# 17-938, β- : JCPDS# 17-936) at $2\theta = 43.3°$. The other group (15th and 50th cycles) also exhibited a similar XRD pattern in each case over the whole scan range. Two electrodes commonly showed typical (311) and (440) peaks of the $LiFe_5O_8$ phase with an additional tetragonal (β- or γ-) $LiFeO_2$ phase ($I4_1/amd$, β-: a = 4.152 Å, c = 4.92 Å, or γ-: a = 4.057 Å, c = 8.759 Å). The intensity of the tetragonal $LiFeO_2$ phase increased as the cycling proceeded. Based on these results, we found that the $Li/Li_xFe_yO_z$ cell showed fairly large capacity fading in the early stage, which seemed to result from the spinel transformation. After the 10th cycle, however, the $Li/Li_xFe_yO_z$ cell presented a very stable cycling characteristic, due to the appearance of the tetragonal $LiFeO_2$ phase; perhaps this might play an important role in maintaining the good cy-

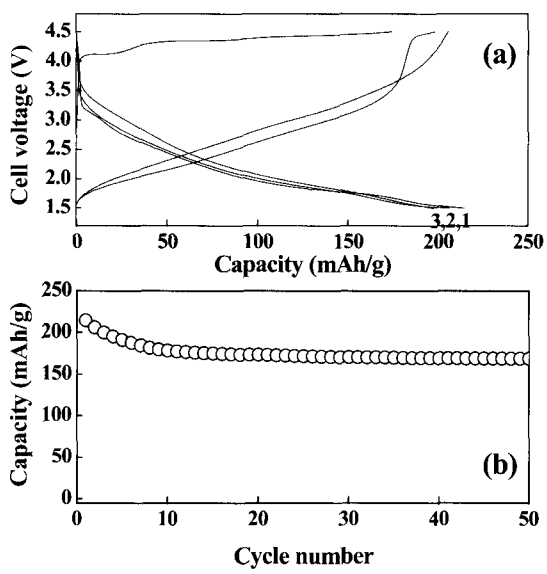

Fig. 9 (a) Charge/discharge curves, (b) specific discharge capacity vs. number of cycles for $Li/Li_xFe_yO_z$ cell obtained at 200℃. The test conditions were a current density of 0.1 mA/cm^2 between 1.5 and 4.5 V at room temperature.

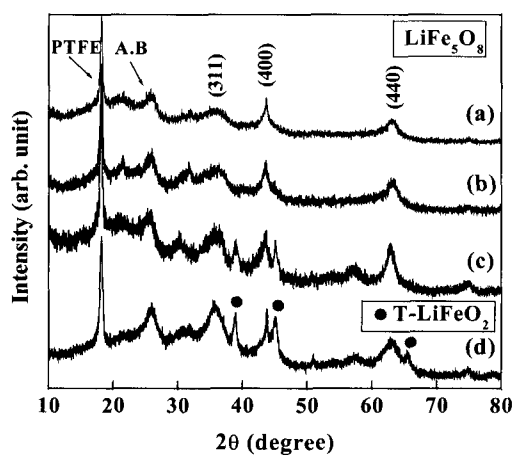

Fig. 10 *Ex-situ* XRD patterns for cycled $Li_xFe_yO_z$ electrodes obtained at 200℃. (a) 1st cycle, (b) 3rd cycle, (c) 15th cycle, and (d) 50th cycle.

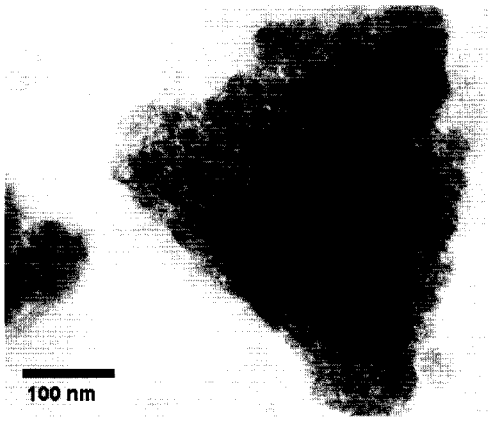

Fig. 11 TEM bright-field image of $Li_xFe_yO_z$ electrode after 50th cycle.

cling retention of this system.

A similar structural change on cycling has already been described for the orthorhombic Li/$LiFeO_2$ system, which showed an almost complete conversion to the $LiFe_5O_8$ spinel phase after 50 cycles. However, one unique characteristic of the Li/$Li_xFe_yO_z$ cell in this study was its tendency to undergo a structural change to the cubic spinel $LiFe_5O_8$ during the early stage and another structural change from the spinel to the tetragonal $LiFeO_2$ phase. The structural change continues even after long-term cycling and results in a mixed phase of spinel $LiFe_5O_8$ and tetragonal $LiFeO_2$ after 50 cycles.

In order to reveal this unique structural change in a different way, TEM analysis was conducted on the same electrodes which were measured by *ex-situ* XRD and was shown in Fig. 11. However, unfortunately, we failed to obtain good results, which could clearly reveal the structural changes from the 1st cycle to 50th cycle; these materials are originally an amorphous phase with a very small nano-particle size (20-40 nm) and the particles are seriously broken due to the lithium insertion/extraction during long-term cycling. We only confirmed that the main structure of the electrode after 50 cycles is very similar to that of the tetragonal β-$LiFeO_2$ phase using TEM analysis. We also still have no concrete proof regarding why nano-crystalline lithium iron oxide partially transforms into the tetragonal $LiFeO_2$ phase and what is the role of the tetragonal phase to improve the cycling performance of the Li/$Li_xFe_yO_z$ system. It is speculated that the tetragonal $LiFeO_2$ phase may contribute to the stabilization of the host material by playing the role of a buffer after spinel transformation in the early stage.

4 Conclusions

Orthorhombic $LiFeO_2$ was synthesized at 150℃ using a solid-state method. The Li/$LiFeO_2$ cell presented not only a high initial capacity of over 150 mAh g^{-1} but also a fairly good cycle retention of 73% after 50 cycles. We first found that the orthorhombic phase of the $LiFeO_2$ material underwent a structural change to the spinel phase during the first cycle and was developed into the well-formed cubic $LiFe_5O_8$ spinel structure during the following cycle. A TEM analysis revealed that a clear spinel $LiFe_5O_8$ phase was found in the electrode after the 3rd cycle and that there was no big difference compared with that of the electrode after 50 cycles. This means that the structural change into the spinel in the Li/*o*-$LiFeO_2$ cell was almost complete during the first cycle, which might be the main reason for the abrupt capacity loss of the Li/*o*-$LiFeO_2$ cell during the early stage. $Li_xFe_yO_z$ with an amorphous structure was synthesized by the conventional solid-state method at 200℃. It showed a high initial discharge capacity (215 mAh g^{-1}) and excellent capacity retention at room temperature, although it exhibited a gradual capacity decrease up to the 10th cycle. This revealed that lithium iron oxide obtained at 200℃ partially transforms into the tetragonal β-$LiFeO_2$ phase after transformation for the spinel $LiFe_5O_8$ in the early stage, which might contribute to the stabilization of the host structure.

Acknowledgments

The authors gratefully acknowledge the financial support by the High-Tech Research Center Project from the Ministry of Education, Culture, Sports, Science and Technology. This work is also partially supported by the Ministry of Science and Technology of the Korean Government (2005).

References

1) K. Mizushima, P. C. Jones, P. J. Wiseman, and J. B. Goodenough, *Mater. Res. Bull.*, **15**, 783 (1980).
2) J. R Dahn, U.Von Sacken, and C. A. Michel, *Solid State Ionics*, **44**, 87 (1990).
3) T. Ohzuku, A. Ueda, and M. Nagayama, *J. Electrochem. Soc.*, **140**, 1862 (1993).
4) H. Arai, S. Okada, Y. Sakurai, and J. Yamaki, *Solid State Ionics*, **95**, 275 (1997).
5) L. Croguennec, P. Deniard, R. Brec, and A. Lecerf, *J. Mater. Chem.*, **5**, 1919 (1995).
6) Y. I. Jang, B. Huang, H. Wang, D. R. Sadoway, and Y. M. Chiang, *J. Electrochem. Soc.*, **146**, 3217 (1999).
7) R. Kanno, T. Shirane, Y. Kawamoto, Y. Takeda, M. Takano, M. Ohashi, and Y. Yamaguchi, *J. Electrochem. Soc.*, **143**, 2435 (1996).
8) T. Shirane, R. Kanno, Y. Kawamoto, Y. Takeda, M. Takano, T. Kamiyama, and F. Izumi, *Solid State Ionics*, **79**, 227 (1995).
9) M. Tabuchi, K. Ado, H. Sakaebe, C. Masquelier, H. Kageyama, and O. Nakamura, *Solid State Ionics*, **79**, 220 (1995).
10) M. Tabuchi, C. Masquelier, T. Takeuchi, K. Ado, I. Matsubara, T. Shirane, R. Kanno, S. Tsutsui, S. Nasu, H. Sakaebe, and O. Nakamura, *Solid State Ionics*, **90**, 129 (1996).
11) K. Ado, M. Tabuchi, H. Kobayashi, H. Kageyama, O. Nakamura, Y. Inaba, R. Kanno, M. Takagi, and Y. Takeda, *J. Electrochem. Soc.*, **144**, L 177 (1997).
12) M. Tabuchi, S. Tsutsui, C. Masquelier, R. Kanno, K. Ado, I. Matsubara, S. Nasu, and H. Kageyama, *J. Solid State Chem.*, **140**, 159 (1998).
13) M. Tabuchi, K. Ado, H. Kobayashi, I. Matsubara, H. Kageyama, M. Wakita, S. Tsutsui, S. Nasu, Y. Takeda, C. Masqulier, A. Hirano, and R. Kanno, *J. Solid State Chem.*, **141**, 554 (1998).

14) Y. Sakurai, H. Arai, S. Okada, and J. Yamaki, *J. Power Sources*, **68**, 711 (1997).
15) Y. Sakurai, H. Arai, and J. Yamaki, *Solid State Ionics*, **113-115**, 29 (1998).
16) T. Ohzuku, A. Ueda, and T. Hirai, *Chemistry Express*, **7**, 193 (1992).
17) J. N. Reimers, E.W. Fuller, E. Rossen, and J. R. Dahn, *J. Electrochem. Soc.*, **140**, 3396 (1993).
18) J. Kim and A. Manthiram, *J. Electrochem. Soc.*, **146**, 4371 (1999).
19) Y.S. Lee, C.S. Yoon, Y.K. Sun, K. Kobayakawa, and Y. Sato, *Electrochem. Commun.*, **4**, 727 (2002).
20) Y.S. Lee, S. Sato, M. Tabuchi, C.S. Yoon, Y.K. Sun, K. Kobayakawa, and Y. Sato, *Electrochem. Commun.*, **5**, 549 (2003).
21) Y.T. Lee, Y.S. Lee, Y. Sato, and Y.K. Sun, *Electrochemistry*, **71**, 1042 (2003).
22) Y. Sato, T. Koyano, M. Mukai, and K. Kobayakawa, *Denki Kagaku* (*Electrochemistry*), **66**, 1215 (1998).